Gold nanoparticles as absolute nano-thermometers

Aquiles Carattino, Martín Caldarola, and Michel Orrit*

Huygens-Kamerlingh Onnes Lab, 2300RA Leiden, The Netherlands

E-mail: orrit@physics.leidenuniv.nl

Abstract

Nano-thermometry is a challenging field that can open the door to intriguing questions ranging from biology and medicine to material sciences. Gold nanorods are excellent candidates to act as nanoprobes because they are reasonably bright emitters upon excitation with a monochromatic source. Gold nanoparticles are commonly used in photothermal therapy as efficient transducers of electromagnetic radiation into heat. In this work we show that the spectrum of the anti-Stokes emission from gold nanorods irradiated in resonance can be used to measure the *absolute temperature* of the nanoparticles and their surrounding media *without* the need of a previous calibration. We show a 4 K accuracy for the determination of the temperature of the sorrounding media with 6 spectral measurements of 180 sec integration time. This procedure can be easily implemented in any microscope capable of acquiring emission spectra and it is not limited to any specific shape of nanoparticles.

Keywords

Gold nanorods, Plasmon, Anti-Stokes, Sensing, Temperature

Most physical, chemical and biological processes depend on temperature. Together with the miniaturization of devices and the advent of nanotechnology the need for measuring temperature with high spatial accuracy started to emerge. Notably in biology[1,2] and medicine[3] measuring and controlling temperature at a sub-cellular scale are the challenge that needs to be overcome to achieve a better understanding of the mechanisms involved in new therapies such as photothermal tumor ablation[4] or controlled drug delivery.[5,6]

Nanometer-size probes with distinctive spectral features are ideal candidates for temperature measurements since they provide high spatial accuracy while far-field optics allow a non-contact readout. Some of the proposed strategies include structures that undergo a conformational change upon an increase in temperature,[7] thus inducing variations in fluorescence intensity of a dye molecule embedded into them.

Also cleverly designed lanthanide-based fluorescent probes in which the ratio of particular emission peaks depends on temperature allow a high accuracy and can be used as nanothermometers[8] even in biological samples.[9] Photobleaching is often an important limitation of these approaches. Recently, Surface Enhanced Raman Spectroscopy (SERS) allowed to measure spectral changes induced by temperature down to single molecules,[10] but a careful calibration of the measurements is crucial.

Gold nanoparticles continue to receive a fair amount of attention because of their unique optical properties.[11] The collective oscillation of conduction electrons, also known as plasmon, shows a resonance in the visible to near infra-red wavelengths. This resonance can be tuned by changing the shape of the particles[12] and is responsible for a large absorption and scattering cross section at the resonance wavelength. These cross sections can be calculated by solving the Maxwell equations numerically employing different computer packages,[13–15] obtaining a good agreement between calculations and what is experimentally achievable.

Thanks to the high absorption and scattering cross section (several times higher than the geometrical cross section) it is relatively simple to detect nanoparticles in a dark-field scattering configuration[16] or via photothermal imaging.[17,18] Alternatively, detecting gold

nanoparticles through their luminescence[19] is also possible; their low quantum yield,[20–23] in the between 10^{-6} and 10^{-5}, is compensated by the enhanced cross section at the surface plasmon resonance (SPR). The luminescence signal is stable over time; gold nanoparticles do not blink nor bleach, therefore are useful labeling agents for processes that require extended periods of observation.[24]

Different metallic nano-objects are being introduced as agents for photothermal therapy[5,25] or drug delivery.[26] One of the advantages of gold nanoparticles is the possibility of tuning their resonance to the near infra-red range, where the penetration of light into tissues can be of several centimeters.[3–5,25,27,28] Moreover the particles can be used not only for treatment, but also for imaging.[5,29] In the case of photothermal therapy, nanoparticles are used as heat sources[4,27] to locally increase the temperature in order to induce the death of specific cells in a tissue.[5,25] However, the temperatures reached[30] can only be estimated from models[29] or from an ad-hoc calibration. Therefore a method that allows simultaneously to increase and to monitor the local temperature will be of great interest in a broad range of fields. In this paper we show that the anti-Stokes luminescence of single gold nanorods can be used to measure their temperature upon resonant CW-mild irradiation. The error is less than 10 K with an acquisition time of 180 sec; with a set of such measurements, the temperature of the surrounding media can be determined with 4 K accuracy or better.

Luminescence of metallic nanoparticles has been the subject of extensive study in recent years. Since the first observation of luminescence from bulk gold,[31] different groups have tried to quantitatively describe the observed properties[32,33] [34–36], such as the quantum yield[20–23,37] and the emission spectrum.[38] In particular, gold nanorods present two distinct resonance energies, namely the transverse and the longitudinal plasmon resonances. These particles can therefore be excited efficiently at one of those energies; the transverse resonance corresponds to a wavelength of about 530 nm and will give rise to a broad luminescence emission with a peak at the longitudinal plasmon energy. Conversely it is possible to excite the particles with a wavelength matching the longitudinal plasmon resonance. In this case the

excitation benefits from an enhanced absorption cross section, but the emission that overlaps the plasmon resonance will be mostly blocked by the filters needed to prevent direct excitation light from reaching the detectors.

In this work, we call 'photoluminescence' any secondary emission? at energies different than from the excitation laser, $\hbar\omega_{\mathrm{L}}$. After virtual or real absorption of an excitation photon, the excited electronic state[31,37] may interact and exchange energy with the phonon bath or, in the case of metals, with the bath of thermal excited charge carriers around the Fermi level. After a variable number of interactions, the excited electronic state will re-emit a photon that can have lower or higher energy than the excitation photon's,[39–41] depending on the interaction. In a non-resonant excitation case, the probability of more than one interaction is negligible and the main contribution to secondary emission is Raman scattering.[34] This is the case for insulators excited well below their electronic absorption edge. In the case of resonant excitation, a long-lived excited state is prepared and has enough time to interact repeatedly with thermal bath, particularly with phonons. This is the case of organic dye molecules or semiconductors, for which relaxed fluorescence will be observed. We also note that fluorescence always present hot bands on the anti-Stokes side of the excitation laser, usually ignored in most fluorescence detection schemes, but far from negligible for heavily doped samples.[42]

Metal nanoparticles fall between these two extremes because the excited electronic state (an electron-hole pair) relaxes very rapidly by interaction of other charge carriers and with phonons. The photoluminescence lifetimes are on the order of tens of femtoseconds.[43] Therefore, there is not enough time to obtain a fully relaxed luminescence, in other words, this photoluminescence is always 'hot'. It is therefore important to realize that Raman scattering, corresponding to the lowes order of interaction with baths, will be an important contribution to this photoluminescence, as it has been proposed earlier.[34,36] However, second and higher orders may also contribute significantly. As all those processes will obey a Boltzman-type relation between anti-Stokes and Stokes emission, they can not be easily distinguished on

the basis of temperature dependence.

The anti-Stokes emission is hihgly sensitive to temperature changes and thus it can be used for thermometry.[44] In this letter we present a simple procedure to extract the absolute temperature from the anti-Stokes photoluminescence spectrum in individual gold nanorods without the need of any temperature calibration. We show that we can determine the particle temperature in-situ with an accuracy of 6% recording a single anti-Stokes spectra (with acquisition time 180s). Moreover, by performing this measurement at different excitation powers we can obtain the temperature of the surrounding media of the nanorods with an accuracy better than 2%.

Phenomenological model for the luminescence emission. In a nutshell, we model the luminescence emission as the radiative recombination of electron-hole pairs created by the decay of the plasmon and subject to interaction with thermal baths. Before the recombination, the carriers may interact with the phonon bath a certain number of times and change their energy, leading to secondary light emission at a different energy. The anti-Stokes spectral contribution arises from interactions that increase the energy of the pair, while the Stokes corresponds to the case where the electron looses some energy. Naturally, the emission process will also be enhanced by the plasmon, thus modulating the luminescence spectrum with the plasmon shape. An scheme of these ideas is shown in the supplementary information.

Exciting a gold nanorod whose resonance frequency is ω_{SPR} with a monochromatic beam at that frequency, generates a collective oscillation of the gas of conduction electrons also called a plasmon. The lifetime of this oscillation can be measured in pulsed experiments or estimated from the inverse of the linewidth and is in the order of 10 fs[43,45] (neglecting any dephasing time T_2^*). The plasmon decays by forming a pair of hot electron and hole with an internal energy equal to the exciting phoyon energy,[46–48] i.e. $E_{e-h} = \hbar\omega_{\mathrm{L}}$.

This hot electron and hole have a small probability of recombining radiatively, i.e. of re-emitting their high electronic energy as a photoluminescence photon. If they have in-

teracted only with static surfaces, their energy will be the same and therefore the emitted photon will have the same energy as the incoming photon, and will not contribute to the measured photoluminescence. It will be blocked by the notch filter used to remove the exciting laser from detection. If, on the other hand, they have interacted with a phonon or a thermally excited electron or hole, they may have lost or acquired energy. In both cases the energy available upon recombination cannot much exceed $\hbar\omega_L + k_\mathrm{B}T$, where k_B represents Boltzmann's constant and T the absolute temperature.

Radiative recombination gives rise to weakly emitting sources spectrally and spatially distributed throughout the particle over a broad frequency band with an exponential cutoff at $\hbar\omega_\mathrm{L} + k_\mathrm{B}T$. The weak recombination emission can be greatly enhanced by the surface plasmon resonance, acting as an antenna. With this model the following predictions can be made. Firstly the emission spectrum must follow the plasmon spectrum if the excitation laser is well above the plasmon resonance as shown in Figure 1, green line. If the excitation falls within the plasmon resonance, the spectrum is expected to follow the plasmon spectrum multiplied by a Bose-Einstein statistics factor arising from phonon population (assuming phonon processes to dominate over carrier-carrier interactions). This factor should be proportional to the phonon occupation number $\bar{n}$ for anti-Stokes and $\bar{n}+1$ for Stokes processes, with

$$\bar{n} = \left(\exp\frac{\hbar\Omega}{k_\mathrm{B}T} - 1\right)^{-1}, \tag{1}$$

where $\hbar\Omega$ is the phonon energy. Other statistics are possible for carrier-carrier interactions obeying Fermi statistics, i.e. $n = \left(\exp(\frac{\hbar\Omega}{k_\mathrm{B}T}) + 1\right)^{-1}$, but we choose phonons here.[34,36]

With this model, it can also be predicted that the emission should be polarized; for the longitudinal plasmon of gold nanorods this polarization coincides with the longitudinal axis of the particle.[49] Moreover, the lifetime should be determined by the lifetime of hot electrons and holes and should be significantly shorter than the thermalization time of the carriers. If this was not the case, a few interactions would be enough to reduce the carriers' energy and

therefore the electron and hole wouldn't have enough energy to produce an optical photon. Finally, only the presence of hot carriers is required in the model. One important assumption for this model is that the coupling mechanism of electron-hole pairs with the plasmons is flat within the plasmon energy band. Therefore excitation well above the plasmon resonance should excite the electron-hole pairs with nearly the same efficiency as just above the plasmon resonance.[23,36]

Application to nanothermometry. According to the model just described, the anti-Stokes emission spectra follows the following form,

$$I(\omega) = \mathrm{I_{SPR}}(\omega) \cdot \left(\exp \frac{\hbar(\omega - \omega_{\mathrm{L}})}{k_{\mathrm{B}} T} - 1 \right)^{-1} \tag{2}$$

where $I(\omega)$ is the emitted intensity, ω is the angular frequency of the photons and ω_{L} is the frequency of the laser. $\mathrm{I_{SPR}}(\omega)$ is the surface plasmon resonance that can be obtained by exciting the particle at energies higher than the resonance. The only remaining free parameter is the temperature T (plus an irrelevant normalization constant not included in eqn. 2.) Clearly, a fit to the measured spectra with this equation can be done to extract the absolute temperature T.

The procedure we propose to obtain the absolute temperature of gold nanorods form the anti-Stokes luminescence emission from without the need of any previous temperature calibration involves the following steps.

1. Obtain the plasmon resonance spectra of the particle. In our case, we detect the spectra of normal photoluminescence, exciting with a 532nm laser. Then we fit this with a Lorentizan line shape to get $I_{\mathrm{SPR}}(\omega)$ appearing in equation 2.

2. Excite near the longitudinal plasmonic resonance and detect the blue-shifted anti-Stokes emission. In our case we used a 633 nmlaser.

3. Fit this high-energy part of the spectra using equation 2 with T as the *only* free parameter.

We emphasize that our method is not simply using the anti-Stokes to Stokes intensity ratio to obtain the temperature of the particle, as it is commonly done with Raman lines for molecules.[50,51] Because of the strong plasmonic enhancement of the emission, the plasmon resonance must be considered in addition to the Boltzmann factor. This is done in an approximate way using the function $I_{\mathrm{SPR}}(\omega)$ form point 1) in the protocol.

Experimental method. All the measurements in this work were performed with a home-built confocal microscope equipped a spectrometer (Acton 500i) in the emission path. We focused our lasers to a diffraction-limited spot using a $60X$, NA 1.4 oil immersion objective (Olympus) and collected the emitted photons through the same objective. This provided high excitation and collection efficiency. We employed a 532 nm (CNI) laser for characterizing the nanorods' plasmon and a 633 nm HeNe (Thorlabs) to excite the nanorods in resonance. We give more experimental details in the Supplementary Information.

Wet chemically synthesized nanorods[52] with average dimensions of 21 nm $\times$ 50 nm and a plasmon resonance around 650 nm were spin-coated onto clean coverslips, controlling the superficial concentration to obtain individual nanorods with the diffraction-limited optical resolution. In addition, the samples were mounted in a flow cell that allowed us to increase the temperature of the medium up to 60 ^{o}C and to monitor it through a Pt100 resistance thermometer placed 1 mm away from the observation area. More details about the experimental setup are given in the Supplementary Information.

To compensate for the drift of the setup while increasing the temperature, we developed a computer program to continuously track a reference particle. The same program was responsible for recording the temperature and triggering the spectrometer. In this way complete data sets were acquired at different temperatures, including spectra while exciting at 532 nm, at 633 nm with different laser intensities and the temperature measured by the Pt100. A spectrum with 532 nm laser excitation was taken after every cycle to ensure that the particle under study had not reshaped due to higher excitation powers.

The intensity of the lasers was controlled via the voltage applied to an acousto-optic

modulator in the optical path. Six accumulations of 30 s integration time each in the spectrometer were recorded at the same laser intensity. This not only allowed us to lower the noise of the measurements because of a longer exposure time (180 sec in total), but also allowed us to remove bright pixels generated by cosmic rays. Having several accumulations is also useful to monitor changes in the intensity of the spectra during the acquisition itself. These changes can be due to a drift of the setup while measuring or to a reshaping of the particle. If the reshaping was confirmed by comparing the spectra acquired with the 532 nm laser,[53] the measurements where rejected. If the changes in the observed emission spectra were due to drift of the setup, the particular data set was not taken into account. For the purposes of this work the excitation intensity is crucial for characterizing the method; if the particle is not in focus it would result in an overestimation of the excitation power.

Experimental Results. The proposed model for the anti-Stokes emission requires to know the plasmon spectrum ($I_{SPR}(\omega)$ in equation 2) of the particle in order to fit the emission at shorter wavelengths and extract the particle temperature. It has been shown that both scattering and luminescence spectra roughly overlap over a broad range of wavelengths.[22] Therefore exciting gold nanorods with 532 nm allows us to record the longitudinal plasmon spectra, as shown in the green solid curve of Figure 1. The peak was fitted by a single Lorentzian, shown in red in the Figure; the dashed part of the curve is the spectral region that was not considered for the fitting. It has to be recalled that the luminescence spectrum is not a perfect Lorentzian since there is a broadband contribution also observed in bulk gold.[31] This appears as an asymmetry in the emission spectrum, particularly visible for wavelengths smaller than 625 nm. The results of this fitting will be employed for the I_{SPR} function defined in equation 2.

The other curves in Fig. 1 show the luminescence emission of the same nanorod while irradiating with a 633 nm laser at different powers, ranging from 25 μW to 75 μW at the back aperture of the objective. The vertical black line shows the wavelength of the laser. The Stokes part of the spectrum at longer wavelengths than the excitation shows the same

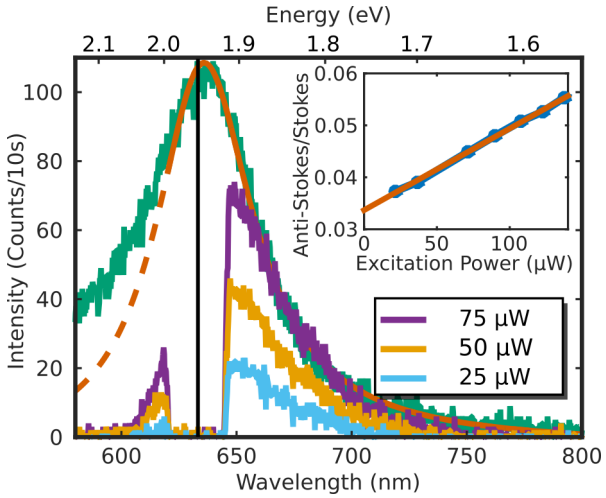

Figure 1: **Luminescence emission spectra of a single gold nanorod.** The green curve is the measured luminescence emission under 532 nm excitation with a Lorentzian fitting in red. The dashed part is the region that was not considered for the fitting. The other curves are the emission of the same particle under 633 nm irradiation at three different powers indicated in the legend. The inset shows the anti-Stokes-to-Stokes ratio as a function of the excitation power, overlapped with a linear fit in red. The dip centered on the laser wavelength is caused by the notch filter used to prevent the excitation laser from reaching the detectors.

shape as the plasmon emission observed under 532 nm excitation, apart from a normalization factor. From the figure it can readily be seen that the shape of the anti-Stokes emission, at shorter wavelengths than excitation, is exponential-like and doesn't follow the Lorentzian shape of the Stokes emission. The dip between Stokes and anti-Stokes is caused by the notch filter that prevents direct excitation light from reaching the detectors.

The inset of Figure 1 shows the anti-Stokes-to-Stokes ratio of the integrated luminescence for different laser excitation intensities. It is possible to see that even with a linear behavior, the anti-Stokes intensity increases more rapidly with laser excitation power than the Stokes emission. We already exploited this phenomenon to image gold nanorods in high-background conditions.[42] Moreover it shows that the anti-Stokes emission depends on laser excitation power slightly differently from its Stokes counterpart. For more information on the power dependence of both the anti-Stokes and Stokes luminescence, please refer to the Supplementary Information.

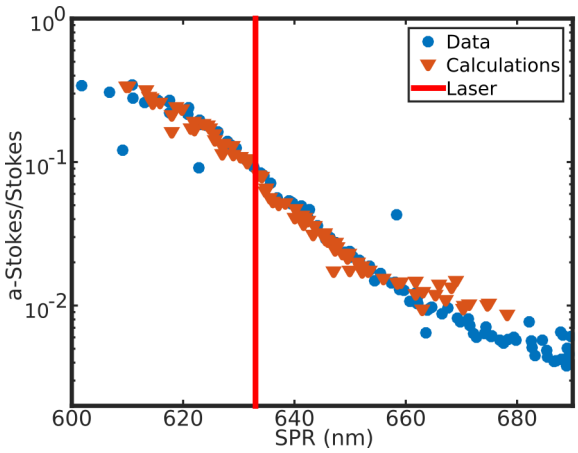

Figure 2: **Characterization of anti-Stokes emission for different SPR.** Ratio of the anti-Stokes to Stokes emission under 633 nm excitation as a function of the resonance wavelength of the particle. The blue circles are experimental results (105 different nanorods), while the red triangles are the results of numerical simulations with equation 1 (82 different nanorods with different aspect ratio). There is a very good agreement between experiment and calculations. Particles with a resonance to the blue of the laser (indicated by the vertical red line) have an increased anti-Stokes emission.

To further characterize this phenomenon, we measured the emission for 105 nanorods with different plasmon resonances under the same 633 nm excitation and calculated the ratio of integrated anti-Stokes to Stokes emission. Figure 2 shows the experimental results in blue circles, where the horizontal axis of the figure is the surface plasmon resonance (SPR) of each particle. The vertical red line marks the laser wavelength. The particles shown in the plot had resonances between 600 nm and 690 nm; the ones showing the maximum ratio of anti-Stokes to Stokes are those with a resonance to the blue of the laser. For these particles the longitudinal plasmon is enhancing preferably the anti-Stokes emission. For particles with a resonance at the laser wavelength the anti-Stokes and the Stokes emission have similar enhancement and show a ratio close to 10%.

Figure 2 also shows the results of numerical calculations following the protocol presented before as the red triangles. An excellent overlap between the measured and the calculated data can be observed. The absorption cross section of 82 particles was calculated numerically with the ADDA package[14] using a fixed width of 23 nm and different lengths to achieve different SPR wavelengths. In the Supplementary material we show the TEM images from

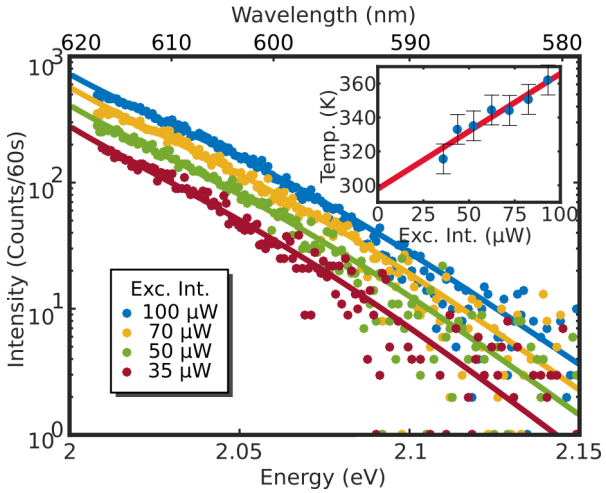

Figure 3: **Anti-Stokes emission at different irradiation powers.** We used the model from equation 2 to fit the experimental data. There is an excellent agreement between data and model. The inset shows the extracted temperature at each power (blue dots) and a linear extrapolation of the data to 0 μW excitation power. The value obtained for room temperature was 293 K while the measured value was 296 K.

which we extracted the size of the nanorods. Each calculated absorption spectrum was fitted by a Lorentzian and used as $I_{SPR}(\omega)$ in eqn. 2. Assuming a diffraction-limited laser spot and using the calculated absorption cross section allowed us to calculate the temperature of the particle. This value was used in eqn. 2 to compute the anti-Stokes emission spectrum. The Stokes emission was set proportional to the excitation power with a shape given by the calculated absorption spectra. Since both anti-Stokes and Stokes emissions are proportional to the excitation power, this term cancels out when computing the ratio. The laser power therefore only enters into the equation when calculating the temperature of the particles. It is remarkable that the agreement between data and calculations was achieved without free parameters, solely taking into account the transmission spectra of the filters.

Furthermore, by fitting the anti-Stokes part of the spectra shown in Figure 1 with equation 2 it is possible to extract the temperature of the particle at each excitation power. Figure 3 shows the results of this procedure. The spectra shown were recorded at 4 different excitation intensities while the full lines are the fits; again, there is an excellent agreement between data and model. For every anti-Stokes measurement we have also acquired the

full plasmon spectrum while exciting with a 532 nm laser before and after the temperature extraction. The full plasmon spectrum is necessary to calculate the parameters of $I_{\mathrm{SPR}}(\omega)$ from equation 2 and also to verify that the particle did not reshape while being excited at resonance.

The inset in Figure 3 shows the temperatures resulting from the fits at different irradiation intensities (blue dots). It has to be noted that the absolute temperatures of the particle at each excitation power were calculated without any calibration. As expected, the temperature of the nanorod is proportional to the excitation intensity, or equivalently to the absorbed energy. Thus, this method provides an *in situ* way to measure the temperature reached by nanoparticles when they are excited with resonant monochromatic light. Additionally, from these data sets it is also possible to calculate the temperature at 0 μW excitation power, i.e. room temperature, by extrapolating the results with a linear fit. The value we obtained in this case is 293 ± 6 K, while room temperature was 296 K, a 2% accuracy.

The accuracy of the obtained temperature depends to a great extent on an accurate modeling of the photoluminescence. The first step in the fitting procedure is the determination of the term $I_{\mathrm{SPR}}(\omega)$ in equation 2. This is achieved by fitting a Lorentzian to the emission spectrum obtained while irradiating with a 532 nm laser. In figure 1 it is possible to observe that the emission spectrum is not perfectly Lorentzian and therefore the fitting results will be sensitive to the portion of the spectrum selected. Depending on the wavelength range selected, the parameters of the Lorentzian fit (its width and peak position) can slightly change therefore giving rise to different temperatures when fitting the anti-Stokes emission spectrum. For a more detailed discussion about the errors for the temperature determination, see the Supplementary Information.

Equation 2 shows that when the resonance is to the red of the laser, the term $I_{\mathrm{SPR}}(\omega)$ will slowly vary in the region where the anti-Stokes emission is observed. Therefore small changes in the parameters of the Lorentzian fit will have a small effect on the temperature extracted. However, particles that are not in resonance with the excitation laser will present

a lower emission due to a smaller absorption cross section and to a lower enhancement of the anti-Stokes emission (see for example figure 2). The error bar in figure 3 and in the following figures is the result of the estimation of the temperature uncertainty because of variations in the plasmon resonance fit. We should mention that there are different strategies to improve this point. For example, longer integration times for the spectra should lead to a better signal to noise ratio and thus a better fit. Another possible way to improve this point is to measure $I_{\mathrm{SPR}}(\omega)$ using another technique, for example dark-field spectroscopy, which gives access to the scattering plasmonic resonance. In this case, one should neglect the shift between absorption and scattering spectra, which is compensated by a better fitting of the plasmonic resonance with a Lorentzian. Alternatively, the use of a narrower notch filter to remove laser light from the detection will give more signal maybe the posibility to test whether Fermi or Bose statistics should be used for the modeling $\left(\exp(\frac{\hbar\Omega}{k_{\mathrm{B}}T}) \pm 1\right)^{-1}$.

As expected from the model, the anti-Stokes emission should depend not only on the particle's intrinsic properties but also on the temperature of the surrounding medium.[54] In order to test this point, we changed the temperature of the sample in a controlled manner and recorded the luminescence emitted by a single nanorod.

For this set of experiments we employed an air objective ($60X$, NA 0.9, Olympus) to avoid the presence of a heat sink directly in contact with the observed area. We employed higher laser powers to compensate for the lower excitation efficiency. At each temperature 7 spectra were acquired at different 633 nm excitation powers and also a spectrum of the plasmon before and after each measurement in order to monitor any possible reshaping of the particles during the experiment.

Figure 4 shows the extracted temperature of a particle at varying excitation powers and at different water temperatures. The blue squares are the results of the measurement at 20 ^{o}C, while the green crosses are measured at 40 ^{o}C and the yellow circles at 60 ^{o}C. The full lines are the calculated temperatures for a particle with plasmon overlapping the measured one and assuming a diffraction-limited focus spot. For the dimensions of the particle, the mean

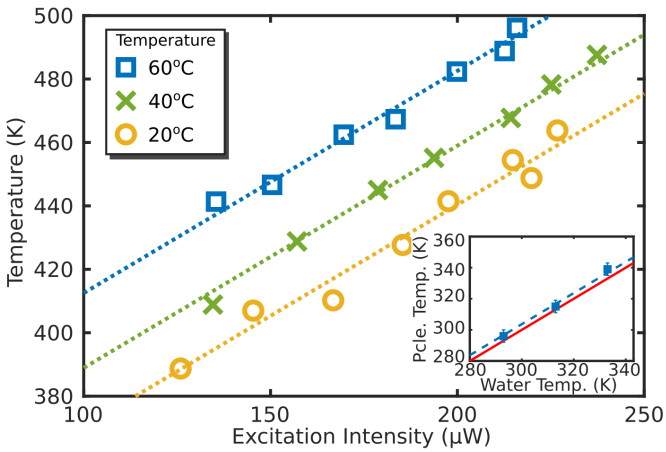

Figure 4: **Calibration-free temperature measurement.** Anti-Stokes-luminescence extracted temperatures for an individual nanorod at different excitation powers and at different sample temperatures. The dashed lines lines are fits with the same slope for the three temperatures. The circles in the inset plot show the local temperature of the sample obtained by extrapolating temperature at zero excitation power as a function of the water temperature. The red line represents the expected curve if both temperatures are identical (equal). The dashed blue line is a fit to the data points with unit slope that shows a systematic offset of 3.8 K, a 1.2% difference.

values from TEM images were used and the length was adjusted to obtain the measured resonance. There is a remarkable agreement between the calculation and the measured values. Moreover it is possible to extrapolate the temperature at zero excitation power for each case as was explained earlier. The results are shown in the inset of the figure for each temperature. The red line with slope 1 is a guide to the eye.

Figure 4 clearly shows that the extracted temperature varies with the temperature of the surrounding medium. More strikingly the method does not require any previous calibration nor adjustment. The values obtained with the extrapolation to 0 μW excitation power were 296 ± 4 K, 315 ± 4 K and 339 ± 4 K for water temperatures of 293 K, 313 K and 333 K respectively. The inset plot in figure 4 presents these points and a red solid line with the expected curve if both temperatures are identical. The dashed line shows a fit of the data that evidences a small systematic offset of 3.8 K. This represents an inaccuracy of 1.2% which is a good result for a calibration-free method. Notably, the presented calibration-free procedure would allow us to perform the same measurements in any other setup and could

act as a reference for calibration of other nano thermometers.

Being able to control and monitor temperature at the nanoscale is of utmost importance in different fields ranging from photothermal therapy[5] to nano fabrication.[55] In this work we have shown a simple procedure that allows us to measure the temperature of single gold nanorods irradiated by a monochromatic continuous laser and without any previous calibration. The level of accuracy of the temperature measurement depends on several factors, but for nanorods it can be estimated to be better than 6 K without any previous calibration.

The model employed for describing the anti-Stokes emission takes into account the plasmon, responsible for enhancing the emission, as well the electron-hole pairs interaction with the thermal baths, where coupling to phonons is the dominant process. We have shown that the correct characterization of the plasmonic resonance is fundamental for the proper extraction of temperature, specially in cases where the resonance is to the blue of the excitation wavelength.

Particles with a resonance to the red of the excitation wavelength would be more reliable in the temperature extraction procedure, but would also exhibit a lower emission towards shorter wavelengths. The trade-off between both effects and the possibility to fully characterize the plasmon resonance, will determine the specific particles that are better suited for each application.

A possible improvement for this technique would be the use nanostructures with a narrow shape distribution such as gold bipyramids.[56] Such structures would be ideal candidates for temperature extraction since they present negligible size dispersion and thus their plasmon can be measured in bulk or determined from theory, avoiding the need of a second excitation source. This would reduce the main source of inaccuracies for the method.

The proposed method doesn't require any calibration, since the only free parameter of the model is the absolute temperature of the nanoparticle under study. Moreover the recording of the anti-Stokes spectrum is readily achievable in any confocal microscope with a coupled

spectrometer. A 6 K accuracy may suffice for several applications; it is important to point out that this value can be improved in different ways: by carefully selecting the particles that show the most favorable plasmon resonance; by determining the plasmon resonance through white-light scattering, avoiding the uncertainty in the fit; by increasing the exposure times to increase the signal-to-noise ratio.

The authors declare no competing financial interest.

Acknowledgement

This work has been financed by FOM, which is part of the Netherlands Organisation for Scientific Research (NWO) (programme number 11SGC02) and by NWO (grant ECHO 712.013.003).

Supporting Information Available

The Supporting Information is available free of charge on the ACS Publications website with the following sections:

- Section: Anti-Stokes emission form gold nanorods
- Section: Experimental setup
- Section: Gold nanorods sample characterization
- Section: Determination of the error in the temperature extraction
- Section: Gold Nanorod temperature numerical calculations

References

(1) Yang, J.-M.; Yang, H.; Lin, L. *ACS Nano* **2011**, *5*, 5067–5071.

(2) Hrelescu, C.; Stehr, J.; Ringler, M.; Sperling, R. A.; Parak, W. J.; Klar, T. A.; Feldmann, J. *J. Phys. Chem. C* **2010**, *114*, 7401–7411.

(3) Li, Y.; Gobin, A. M.; Dryden, G. W.; Kang, X.; Xiao, D.; Li, S. P.; Zhang, G.; Martin, R. C. G. *Int. J. Nanomedicine* **2013**, *8*, 2153–2161.

(4) Gobin, A. M.; Lee, M. H.; Halas, N. J.; James, W. D.; Drezek, R. A.; West, J. L. *Nano Lett.* **2007**, *7*, 1929–1934.

(5) Huang, X. H.; El-Sayed, I. H.; Qian, W.; El-Sayed, M. a. *J. Am. Chem. Soc.* **2006**, *128*, 2115–2120.

(6) Huo, S.; Jin, S.; Ma, X.; Xue, X.; Yang, K.; Kumar, A.; Wang, P. C.; Zhang, J.; Hu, Z.; Liang, X.-J. *ACS Nano* **2014**, *8*, 5852–5862.

(7) Ebrahimi, S.; Akhlaghi, Y.; Kompany-Zareh, M.; Rinnan, A. *ACS Nano* **2014**,

(8) Liu, X.; Siegler, M. A.; Bouwman, E. *European Journal of Inorganic Chemistry* **2016**, *2016*, 2984–2988.

(9) Vetrone, F.; Naccache, R.; Zamarrón, A.; Juarranz de la Fuente, A.; Sanz-Rodríguez, F.; Martinez Maestro, L.; Martín Rodriguez, E.; Jaque, D.; García Solé, J.; Capobianco, J. A. *ACS Nano* **2010**, *4*, 3254–8.

(10) Pozzi, E. A.; Zrimsek, A. B.; Lethiec, C. M.; Schatz, G. C.; Hersam, M. C.; Van Duyne, R. P. *J. Phys. Chem. C* **2015**, *119*, 21116–21124.

(11) Zijlstra, P.; Orrit, M. *Reports Prog. Phys.* **2011**, *74*, 106401.

(12) Carattino, A.; Khatua, S.; Orrit, M. *Phys. Chem. Chem. Phys.* **2016**, *18*, 15619–15624.

(13) Draine, B. T.; Flatau, P. J. *J. Opt. Soc. Am. A* **1994**, *11*, 1491.

(14) Yurkin, M. A.; Hoekstra, A. G. *J. Quant. Spectrosc. Radiat. Transf.* **2011**, *112*, 2234–2247.

(15) Oskooi, A. F.; Roundy, D.; Ibanescu, M.; Bermel, P.; Joannopoulos, J.; Johnson, S. G. *Comput. Phys. Commun.* **2010**, *181*, 687–702.

(16) Hu, M.; Novo, C.; Funston, A.; Wang, H.; Staleva, H.; Zou, S.; Mulvaney, P.; Xia, Y.; Hartland, G. V. *J. Mater. Chem.* **2008**, *18*, 1949.

(17) Boyer, D.; Tamarat, P.; Maali, A.; Lounis, B.; Orrit, M. *Science* **2002**, *297*, 1160–1163.

(18) Berciaud, S.; Lasne, D.; Blab, G.; Cognet, L.; Lounis, B. *Phys. Rev. B* **2006**, *73*, 045424.

(19) Tcherniak, A.; Dominguez-Medina, S.; Chang, W. S.; Swanglap, P.; Slaughter, L. S.; Landes, C. F.; Link, S. *J. Phys. Chem. C* **2011**, *115*, 15938–15949.

(20) Fang, Y.; Chang, W.-S.; Willingham, B.; Swanglap, P.; Dominguez-Medina, S.; Link, S. *ACS Nano* **2012**, *6*, 7177–84.

(21) Rao, W.; Li, Q.; Wang, Y.; Li, T.; Wu, L. *ACS Nano* **2015**, *9*, 2783–2791.

(22) Yorulmaz, M.; Khatua, S.; Zijlstra, P.; Gaiduk, A.; Orrit, M. *Nano Lett.* **2012**, *12*, 4385–91.

(23) Cheng, Y.; Lu, G.; He, Y.; Shen, H.; Zhao, J.; Xia, K.; Gong, Q. *Nanoscale* **2016**, *8*, 2188–2194.

(24) Wang, H.; Huff, T. B.; Zweifel, D. A.; He, W.; Low, P. S.; Wei, A.; Cheng, J.-X. *Proc. Natl. Acad. Sci.* **2005**, *102*, 15752–15756.

(25) Huang, X.; Jain, P. K.; El-Sayed, I. H.; El-Sayed, M. A. *Lasers Med. Sci.* **2008**, *23*, 217–228.

(26) Kang, B.; Afifi, M. M.; Austin, L. a.; El-Sayed, M. a. *ACS Nano* **2013**, *7*, 7420–7.

(27) Hirsch, L. R.; Stafford, R. J.; Bankson, J. A.; Sershen, S. R.; Rivera, B.; Price, R. E.; Hazle, J. D.; Halas, N. J.; West, J. L. *Proc. Natl. Acad. Sci. U. S. A.* **2003**, *100*, 13549–54.

(28) O'Neal, D.; Hirsch, L. R.; Halas, N. J.; Payne, J.; West, J. L. *Cancer Lett.* **2004**, *209*, 171–176.

(29) Zhao, T.; Yu, K.; Li, L.; Zhang, T.; Guan, Z.; Gao, N.; Yuan, P.; Li, S.; Yao, S. Q.; Xu, Q.-H.; Xu, G. Q. *ACS Appl. Mater. Interfaces* **2014**, *6*, 2700–2708.

(30) Donner, J. S.; Thompson, S. a.; Alonso-Ortega, C.; Morales, J.; Rico, L. G.; Santos, S. I. C. O.; Quidant, R. *ACS Nano* **2013**, *7*, 8666–8672.

(31) Mooradian, A. *Phys. Rev. Lett.* **1969**, *22*, 185–187.

(32) Mohamed, M. B.; Volkov, V.; Link, S.; El-Sayed, M. A. *Chem. Phys. Lett.* **2000**, *317*, 517–523.

(33) Beversluis, M.; Bouhelier, A.; Novotny, L. *Phys. Rev. B* **2003**, *68*, 1–10.

(34) Huang, J.; Wang, W.; Murphy, C. J.; Cahill, D. G. *Proc. Natl. Acad. Sci. U. S. A.* **2014**, *111*, 906–11.

(35) Hugall, J. T.; Baumberg, J. J. *Nano letters* **2015**, *15*, 2600–2604.

(36) Mertens, J.; Kleemann, M.-E.; Chikkaraddy, R.; Narang, P.; Baumberg, J. J. *Nano Letters* **2017**, *17*, 2568–2574.

(37) Dulkeith, E.; Niedereichholz, T.; Klar, T.; Feldmann, J.; von Plessen, G.; Gittins, D.; Mayya, K.; Caruso, F. *Phys. Rev. B* **2004**, *70*, 205424.

(38) Link, S.; El-Sayed, M. A. *Int. Rev. Phys. Chem.* **2000**, *19*, 409–453.

(39) Hodak, J. H.; Henglein, A.; Hartland, G. V. *J. Chem. Phys.* **2000**, *112*, 5942–5947.

(40) Giri, A.; Gaskins, J. T.; Foley, B. M.; Cheaito, R.; Hopkins, P. E. *J. Appl. Phys.* **2015**, *117*, 044305.

(41) Arbouet, A.; Voisin, C.; Christofilos, D.; Langot, P.; Fatti, N. D.; Vallée, F.; Lermé, J.; Celep, G.; Cottancin, E.; Gaudry, M.; Pellarin, M.; Broyer, M.; Maillard, M.; Pileni, M. P.; Treguer, M. *Phys. Rev. Lett.* **2003**, *90*, 177401.

(42) Carattino, A.; Keizer, V. I.; Schaaf, M. J.; Orrit, M. *Biophysical journal* **2016**, *111*, 2492–2499.

(43) Link, S.; El-Sayed, M. A. *The Journal of Physical Chemistry B* **1999**, *103*, 8410–8426.

(44) Xie, X.; Cahill, D. G. *Applied Physics Letters* **2016**, *109*, 183104.

(45) Sönnichsen, C.; Franzl, T.; Wilk, T.; von Plessen, G.; Feldmann, J.; Wilson, O.; Mulvaney, P. *Phys. Rev. Lett.* **2002**, *88*, 077402.

(46) Sundararaman, R.; Narang, P.; Jermyn, A. S.; Goddard III, W. A.; Atwater, H. A. *Nature communications* **2014**, *5*.

(47) Brongersma, M. L.; Halas, N. J.; Nordlander, P. *Nat. Nanotechnol.* **2015**, *10*, 25–34.

(48) Manjavacas, A.; Liu, J. G.; Kulkarni, V.; Nordlander, P. *ACS Nano* **2014**, *8*, 7630–7638.

(49) He, Y.; Xia, K.; Lu, G.; Shen, H.; Cheng, Y.; Liu, Y.-c.; Shi, K.; Xiao, Y.-F.; Gong, Q. *Nanoscale* **2015**, *7*, 577–582.

(50) Krishnan, K. *Nature* **1928**, *122*, 650.

(51) Zondervan, R. Single-molecule dynamics at variable temperatures. Ph.D. thesis, Casimir PhD Series, Delft-Leiden, Niels Bohrweg 2, 2333 CA Leiden, The Netherlands, 2006.

(52) Nikoobakht, B.; El-Sayed, M. A. *Chem. Mater.* **2003**, *15*, 1957–1962.

(53) Liu, Y.; Mills, E. N.; Composto, R. J. *J. Mater. Chem.* **2009**, *19*, 2704.

(54) Konrad, A.; Wackenhut, F.; Hussels, M.; Meixner, A. J.; Brecht, M. *J. Phys. Chem. C* **2013**, *117*, 21476–21482.

(55) Fedoruk, M.; Meixner, M.; Carretero-Palacios, S.; Lohmuller, T.; Feldmann, J. *ACS Nano* **2013**, *7*, 7648–7653.

(56) Pelton, M.; Sader, J. E.; Burgin, J.; Liu, M.; Guyot-Sionnest, P.; Gosztola, D. *Nat. Nanotechnol.* **2009**, *4*, 492–495.

Graphical TOC Entry

Some journals require a graphical entry for the Table of Contents. This should be laid out "print ready" so that the sizing of the text is correct.
Inside the `tocentry` environment, the font used is Helvetica 8 pt, as required by *Journal of the American Chemical Society*.
The surrounding frame is 9 cm by 3.5 cm, which is the maximum permitted for *Journal of the American Chemical Society* graphical table of content entries. The box will not resize if the content is too big: instead it will overflow the edge of the box.
This box and the associated title will always be printed on a separate page at the end of the document.